Article

Patterns

VONet: A deep learning network for 3D reconstruction of organoid structures with a minimal number of confocal images

Highlights

- Inefficiencies in conventional 3D structure rendering techniques
- VONet: efficient 3D structure reconstruction of organoids
- Artificially synthesized virtual organoid dataset for training VONet
- Exceptional performance of VONet for predicting organoid 3D structure

Authors

Euijeong Song, Minsuh Kim, Siyoung Lee, ..., Seok Chung, Ji Hun Yang, Tae Hwan Kwak

Correspondence

sidchung@korea.ac.kr (S.C.), jihun.yang@nextandbio.com (J.H.Y.), taehwan.kwak@nextandbio.com (T.H.K.)

In brief

Developing AI-based technologies to analyze three-dimensional structures of organoid models is challenging due to the need for large amounts of data from cultured organoids. To overcome this, the authors created virtual organoids that closely mimic the histological characteristics of real organoids. This approach allowed for the successful training of an AI-based rendering software, VONet, which showed exceptional performance in various analyses.

Song et al., 2024, Patterns *5*, 101063
October 11, 2024
https://doi.org/10.1016/j.patter.2024.101063

CellPress

Patterns

CellPress
OPEN ACCESS

Article

VONet: A deep learning network for 3D reconstruction of organoid structures with a minimal number of confocal images

Euijeong Song,[1] Minsuh Kim,[2] Siyoung Lee,[1] Hui-Wen Liu,[2] Jihyun Kim,[1] Dong-Hee Choi,[2] Roger Kamm,[3,4] Seok Chung,[2,5,*] Ji Hun Yang,[1,*] and Tae Hwan Kwak[1,6,*]

[1]Next&Bio, Seoul, South Korea
[2]School of Mechanical Engineering, Korea University, Seoul, South Korea
[3]Department of Biological Engineering, Massachusetts Institute of Technology, Cambridge, MA 02139, USA
[4]Department of Mechanical Engineering, Massachusetts Institute of Technology, Cambridge, MA 02139, USA
[5]KU-KIST Graduate School of Converging Science and Technology, Korea University, Seoul, South Korea
[6]Lead contact
*Correspondence: sidchung@korea.ac.kr (S.C.), jihun.yang@nextandbio.com (J.H.Y.), taehwan.kwak@nextandbio.com (T.H.K.)
https://doi.org/10.1016/j.patter.2024.101063

THE BIGGER PICTURE Organoids are 3D lab-grown models that mimic the structure of human tissues, making them incredibly useful for etiological research and testing drug effects. Unlike traditional 2D cell cultures, structural characteristics of organoids are more complex and require advanced techniques, many resources, and significant time to analyze accurately. To make this process easier, we developed VONet, a deep learning AI software trained on simulated organoid images. VONet offers a faster and more accurate way to analyze the 3D structure of organoids compared to current methods. This breakthrough helps us better understand organoids, advancing research in medicine and drug development.

SUMMARY

Organoids and 3D imaging techniques are crucial for studying human tissue structure and function, but traditional 3D reconstruction methods are expensive and time consuming, relying on complete z stack confocal microscopy data. This paper introduces VONet, a deep learning-based system for 3D organoid rendering that uses a fully convolutional neural network to reconstruct entire 3D structures from a minimal number of z stack images. VONet was trained on a library of over 39,000 virtual organoids (VOs) with diverse structural features and achieved an average intersection over union of 0.82 in performance validation. Remarkably, VONet can predict the structure of deeper focal plane regions, unseen by conventional confocal microscopy. This innovative approach and VO dataset offer significant advancements in 3D bioimaging technologies.

INTRODUCTION

Organoids are miniature organ-like cell clusters produced by the *in vitro* self-organization of stem cells. They are similar to their *in vivo* counterparts in terms of biological and molecular traits, physiological characteristics, cellular composition, and three-dimensional (3D) architecture.[1] Therefore, organoids are a useful model for studying human development and therapeutics, such as personalized and regenerative medicine.[1] The 3D structure of organoids replicates the biological and physiological states of their corresponding tissues in terms of cellular composition, cell-cell interactions, and microenvironments.[2,3] The specific biological conditions of each tissue can be investigated by observing the morphology and microanatomical structure of organoids.[4] In addition, various extrinsic factors, including signaling molecules in the culture medium, extracellular matrix composition, and physical properties of the hydrogel, can affect the morphology of organoids.[2,5,6] Consequently, how extrinsic factors such as drugs or toxic substances affect the physiological state of organoids may be predicted by observing the morphological changes in organoids over time. For this, systematic studies to investigate how intrinsic cellular and extrinsic factors affect organoid structure determination are essential.

The quantitative characterization of cellular morphology has helped elucidate the function and behavior of the intracellular components associated with tissue development and pathogenesis.[7] Although conventional two-dimensional (2D) image analyses offer valuable information for quantifying biological features in adherent cell cultures, they fail to comprehensively capture the diverse morphological characteristics and structures

of 3D biological models. Furthermore, the utilization of 2D image analysis techniques for classifying and labeling intracellular and extracellular components, such as cytoplasm or nuclei, within the structure of 3D tissues presents several limitations.[5] Confocal fluorescence microscopy is the most widely used optical technique for observing the 3D structures of biological samples. As the pinhole of the confocal microscope eliminates out-of-focus signals by spatially filtering volumetric data, a confocal image displays biological information contained in a single focal plane with minimum ambient interference.[8] Furthermore, advancements in modern computer science have enabled the reconstruction of 3D structures of biological specimens using z stack imaging, a technique that acquires cross-sectional images of biological samples along the z axis using confocal microscopy. This technique also facilitates the quantitative analysis of cellular and intercellular components within 3D tissues.[9] Therefore, the integration of high-resolution single-plane fluorescence imaging techniques, such as confocal microscopy, with 3D image rendering technologies is considered the most rational approach for investigating the structural and physiological characteristics of 3D tissues, including organoids.

Image-based high-content screening (HCS), a recent development in high-throughput screening (HTS), facilitates quantifying various biological features. Given the aforementioned characteristics, organoids hold immense promise as a suitable model for HCS-based discovery of toxicants and therapeutic candidates when optimized for HTS analysis platforms.[10,11] Despite the superior characteristics of organoid models, there are significant challenges that need to be addressed for the commercialization of organoid-based HCS analysis, as most current HTS and HCS analysis platforms primarily utilize 2D cultured cells. The most significant limitation lies in the 3D nature of organoid models, which necessitates the acquisition of multiple z stack images to capture comprehensive information across the entire organoid volume, unlike conventional 2D cell models where single-plane microscopy images suffice for data extraction. Although contemporary 3D bioimaging technology has advanced, obtaining complete z stack images remains time-consuming. For example, reconstructing the 3D structure of a single organoid with a height of 500 μm from 100 single-plane confocal microscopic images along the z axis takes >5 min. While HCS tests are conducted in 96-, 384-, or 1,536-well array formats, obtaining complete single-plane images from such a large number of organoids is exceedingly time-consuming. This inefficiency must be remedied to practically use organoid-based HCS.

As advanced imaging technologies such as HCS have been developed to promptly acquire large numbers of accurate images, a high demand exists for analytical technologies that can classify a large volume of images.[12] Recently, deep learning has exhibited superior performance in numerous disciplines, including biological image processing. Image segmentation is a fundamental prerequisite for accurately quantifying biological images.[13] U-net, a unique deep learning-based segmentation technique devised by Ronneberger et al.,[14] exhibited superior performance over all non-deep learning segmentation algorithms and distinguished objects by modifying the endpoint channel and training the network with appropriate datasets. Current image analysis applications of U-net include cell segmentation research,[15] computed tomography image segmentation,[16] retinal blood vessel identification,[17] and neurite detection.[18] To train deep learning networks, the embedding/diffusion procedure requires a vast quantity of training data. For example, the Stable Diffusion network has been trained on a dataset of 2.3 billion images.[19] Despite the potential of deep learning-powered image analysis techniques to revolutionize biological research, their widespread adoption is hindered by the substantial data requirements; the complexities and costs associated with image acquisition; ethical, safety, and privacy concerns; and the heterogeneity of experimental protocols.

The development of techniques that can significantly reduce the time and resources required for reconstructing the 3D structure of organoids using deep learning could significantly accelerate the commercialization of organoid-based HCS technology, as discussed previously. However, a major hurdle to this advancement lies in the nascent field of deep learning-based organoid analysis. To develop deep learning models, a substantial amount of training images with comprehensive annotations representing specific experimental conditions is required. However, because organoids are a relatively nascent research area, there is insufficient accumulation of image data obtained under consistent experimental conditions, resulting in a critical issue of absolute data scarcity. To address this data scarcity issue, proposals have emerged suggesting the use of synthetic images to replace the massive training datasets typically required for deep learning models. Recently developed artificial intelligence (AI)-based image synthesis techniques may be used to address the issue of insufficient data. Deep learning software, including DALL-E,[20] Midjourney (https://www.midjourney.com/), and novelAI (https://novelai.net/), can generate images from text and perform segmentation and basic object detection. These tools are based on the iterative diffusion of a noise-like image formed from vector-embedded words and sentences. In fact, we used Midjourney to create an image based on the text "bright-field microscopic image of colon cancer organoid," but we obtained results that were different from those obtained through actual experiments (data not shown). It demonstrates that popular generative AI models lack sufficient data to understand organoid structures. For this reason, many challenges remain in deep learning network training for organoid research.

Here, we developed a deep learning-based organoid 3D rendering system to analyze organoid morphology with a minimal number of z stack images to address the fundamental bottleneck of imaging speed, a major hurdle impeding the commercialization of organoid-based HCS. Due to the scarcity of publicly available organoid image datasets specifically designed for structural characterization studies, we created tens of thousands of synthetic virtual organoids (VOs) based on the growth properties of cultured organoids. Our VO data comprised z stack images reflecting random survival rates for each VO. We trained our deep learning network, VONet, using a VO dataset and performed cross-validation. VONet generated a precise 3D structure of a real organoid (RO) from a small number of z stack images, comparable to that constructed using 64 z stack images.

RESULTS

Generation of synthetic VOs

To accurately model the organoid structure using the deep learning network, we investigated organoid morphology and

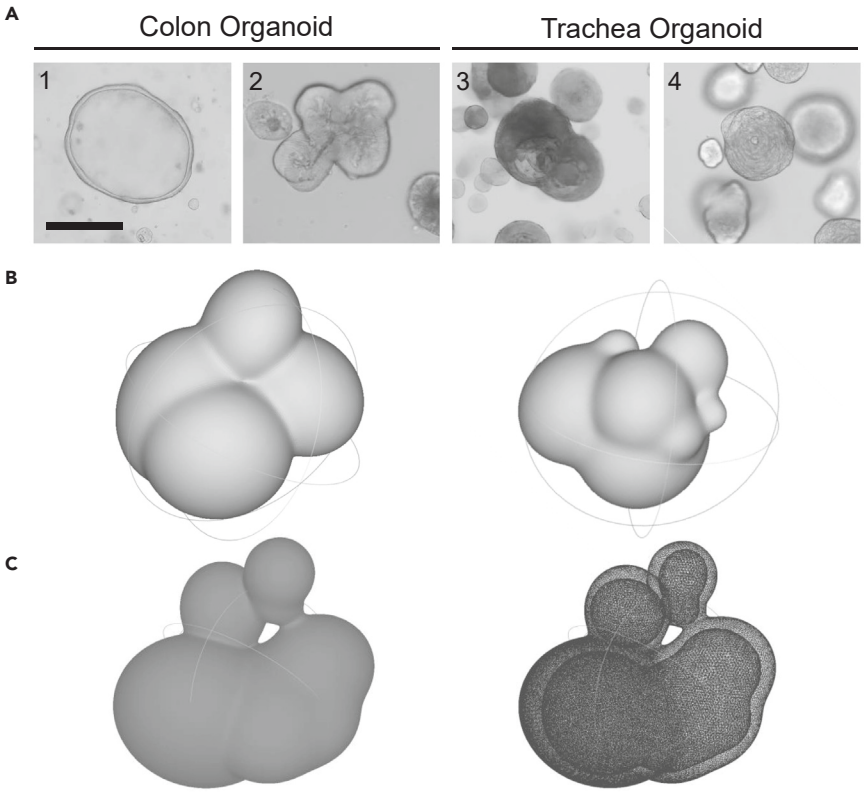

Figure 1. Synthetic VOs simulating the growth pattern of cultured organoids

(A) Bright-field images showing the distinct morphology of the cultured normal colon and cancer organoids compared to tracheal organoids. Scale bar, 200 μm.

(B) The 3D images of the synthetic VOs generated using the VO construction technique. Synthesized VOs comprised multiple ovals that were randomly created.

(C) Perspective drawing showing the internal structure of the VOs. Synthetic VOs comprised a hollow lumen surrounded by thin walls.

growth patterns. Colon organoids show diverse shapes during cultivation[21] compared with other organoids.[22,23] The organoids that we cultured under conventional conditions showed different sizes and shapes (Figure 1A), including thick-walled spherical, budding tubular, thin-walled bubble-like, and compact globular shapes. To identify key characteristics among the various structural features of organoids, we traced the morphological changes during their growth. While growing, superficial lumps with various dimensions and random intruding cavities were formed on the organoids, resulting in organoids with several specific morphologies (Figure S1).

We virtually generated various organoids by considering their morphological changes, including structure, and the intensity values in bright-field images. To reflect the expected growth patterns, multiple ovals were generated and superimposed to mimic randomly generated blobs in organoids (Figures 1B, 1C, and S2). Our VOs also presented some cavities (Figure 1C). We restricted the maximum number of ovals in an organoid to 20 to balance the cost and resolution of the output data. With 50 ovals, the computation took 2,252 s, whereas with 10 ovals, the computation took 47 s. Furthermore, as the number of ovals increases, the additional synthesis time required is significantly increased. However, the morphological changes in the newly endowed organoids are very subtle. With several ovals in a narrow area, overlap will increase, generating a smooth and simple shape while decreasing structural diversity in the dataset (Figure S3A). Furthermore, if the maximum oval radius is too small, the VO would present as scattered ovals with a simplified structure (Figure S3B). We randomly generated 39,466 VOs (50 of them are shown in Figure S2) that simulated the various shapes and sizes of organoids based on experimental growth patterns.

Dataset of synthetic VOs and deep learning network training

The mesh data generated from the VOs were transformed into voxel data. We assumed the location of the nucleus using a 3D shape of the mesh data and synthesized the z stack images with survival rates referred to in the confocal images of ethidium homodimer-1 (EthD-1)-stained organoids. We utilized EthD-1-stained organoid images to incorporate realistic cell death representation into our synthetic images. The nuclei of dead cells within organoids exhibit distinct differences in size and morphology compared to healthy cell nuclei. This characteristic was crucial for our objective of generating synthetic images that accurately reflect the presence of dead cells within the organoid structure. Each VO had a different live/dead rate, which was randomly determined and applied to the nucleus status (Figure 2A). With low survival rates, the organoid border in the z stack images contained dead nuclei (Figure 2A). The dead nuclei were set to fall off from the organoid and randomly float in VOs; this was similar to the behavior of the dead nuclei in cultured organoids (Figure 2B). In conclusion, the morphological information of an organoid completely disappears when the number of live cells is <0.2% of the total number of cells; therefore, the live/dead rate of a VO was randomly set between 1 and 0.2.

VONet, which was designed using a fully convolutional-neural network structure, was trained using three data types in the VO dataset: mesh, voxel, and imaging data (Figure 3A). The input data of the synthetic images comprised 64 layers. Some layers were filled with imaging data and others were blank. We trained VONet using >39,000 VOs to reconstruct the 3D structural data of an organoid from synthetic z stack images. Then, VONet was automatically trained by backpropagation (Figure 3B). We defined the loss function for backpropagation as follows:

$$L = JI + MAE(V_{res}, V_{ans}) \quad \text{(Equation 1)}$$

$$JI = IoU = \frac{V_{intersection}}{V_{union}} = \frac{V_{res} \cap V_{ans}}{V_{res} \cup V_{ans}} = \frac{\sum(V_{res} \circledcirc V_{ans})}{\sum Maximum(V_{res}, V_{ans})} \quad \text{(Equation 2)}$$

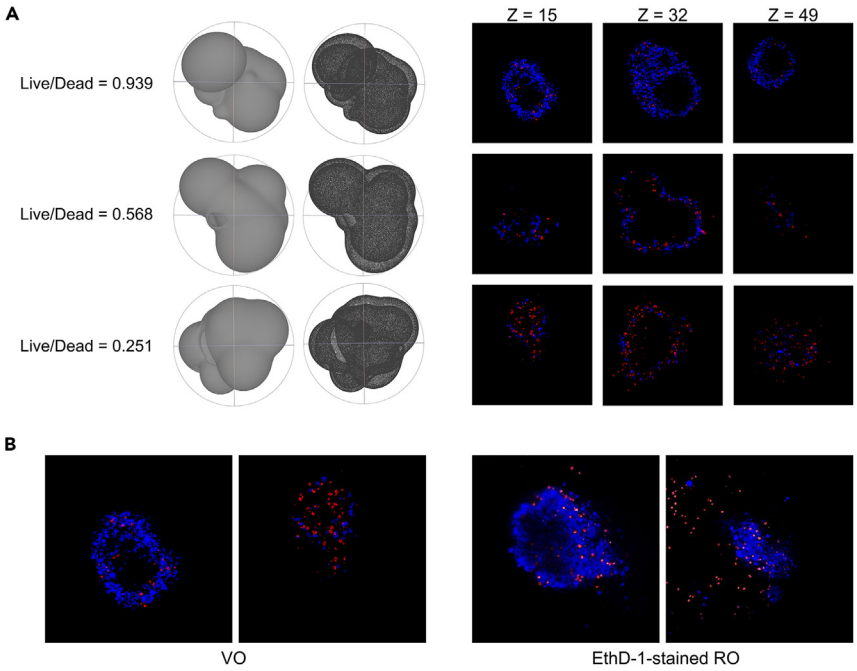

Figure 2. Synthesized VOs with cell survival rate

(A) VO images and their z stack images with cell survival rate values (0.939, 0.538, and 0.251). Based on this input, the nucleus of live cells was stained blue, whereas that of dead cells was stained red.

(B) z Stack images of the VOs (left) and EthD-1-stained ROs (right).

V_{res} is the voxel data derived from VONet. V_{ans} ("answer data") represents 3D voxel data for the VO structure, which is the target data for training. Jaccard index (*JI*), also called the intersection over union (IoU) criterion, is a useful index to measure the performance of image processing algorithms and loss function for deep learning network training. Letting the value of one voxel in V_{res} be v_{1i} and V_{ans} be v_{2i}, the mean absolute error was calculated as $|v_{1i} - v_{2i}|$ ($i \leq n$), where n is the number of voxels in V_{res}. The symbol ◎ denotes the element-wise multiplication of two matrices of the same size (also known as the Hadamard product). Maximum functions choose the larger value from two matrices element-wise. Through these equations, the loss function L indicates by how much the volumetric data in V_{res} and V_{ans} differ. Subsequently, VONet was trained to minimize the value of L. To ensure that VONet is not overfit, we performed 10-fold cross-validation. The IoU score of each fold varies from 0.59 to 0.66 (Table S1). The final output was obtained by leaving only those with a non-zero intensity value in V_{res}.

Application of the deep learning network to an RO dataset

For cross-validation, we established an RO dataset comprising the z stack images of 10 cultured organoids (Figure 4A). Each set contained 64 z stack images. The 3D structural data were generated by simply stacking all data in the z stack images with intensities exceeding the threshold, represented as V_{64} (Figure 4B). The intensity threshold was set to 0.05, an empirically determined value for denoising.

Figure 4B illustrates the 3D structure reconstructed from stacking 64 z stack images (V_{64}) of three ROs, and Figure 4C shows the 3D structure predicted by VONet using n randomly selected 11 z stack images (V_{res}) from the same ROs. As shown by the reconstructed 3D structures of both groups, the 3D structure of the organoid predicted by VONet from 11 single-plane images is strikingly similar to the 3D structure reconstructed by stacking 64 single-plane images (Figures 4B and 4C). Using confocal microscopic z stack imaging, data loss occurs due to the weakened fluorescence signal intensity in the single-plane images located at a deep focal distance (when the z value is >45) (second column of images in Figure 4A). Owing to interference from the structural elements of the organoids located at relatively shallow focal distances, it is exceedingly difficult to capture the fluorescence signals in regions of the sample at deep focal distances (Figure 4A). Since organoids, with their closed structures, exhibit cellular structures even at deep focal distances, the loss of fluorescent signals at deep focal distances is considered a limitation of conventional confocal microscopy-based imaging techniques, particularly when imaging thick tissue samples. Interestingly, while the organoid 3D structures in V_{64} depict all deep focal distance-associated organoid structures as empty spaces, V_{res} predicts and reconstructs the deep focal distance-associated organoid structures. These results underscore the remarkable capability of VONet of not merely reconstructing 3D structures from input data but also of predicting and generating overall desirable 3D organoid structures.

Performance evaluation of the deep learning network using limited organoid image resources

We evaluated the estimation performance of VONet using a limited number of experimentally obtained images in the RO dataset. To ensure a comprehensive interpretation, the performance of VONet was validated using additional indicators (Figure S4): IoU over the whole voxel volume (IoU_{all}), IoU of the corresponding volume (IoU_{corr}, sum of IoU for slices with a non-zero value), and IoU of the bright portion of volume (IoU_{bright}, sum of IoU for slices with z values of $<0.7 \times z_{max}$). As the light source of the confocal microscopy was beneath the organoid, IoU_{bright} was the average IoU value of segments with a z value less than the threshold. From the RO dataset, we selected and placed 3–15 images of each organoid into an input array with the same z axis spacing. Each voxel datum ($V_{res}(k)$) was generated according to the number of images used (indicated by "k"). We analyzed three IoU values by varying k values in 10 cultured organoids (Figures 5A–5C; raw data are shown in Tables 1, 2, and 3). $V_{res}(k)$ computed using VONet with k z stack images of a cultured organoid showed a correlation with V_{64}, as confirmed by the three IoU indices. IoU_{all} reached 74% (0.72 IoU) with only

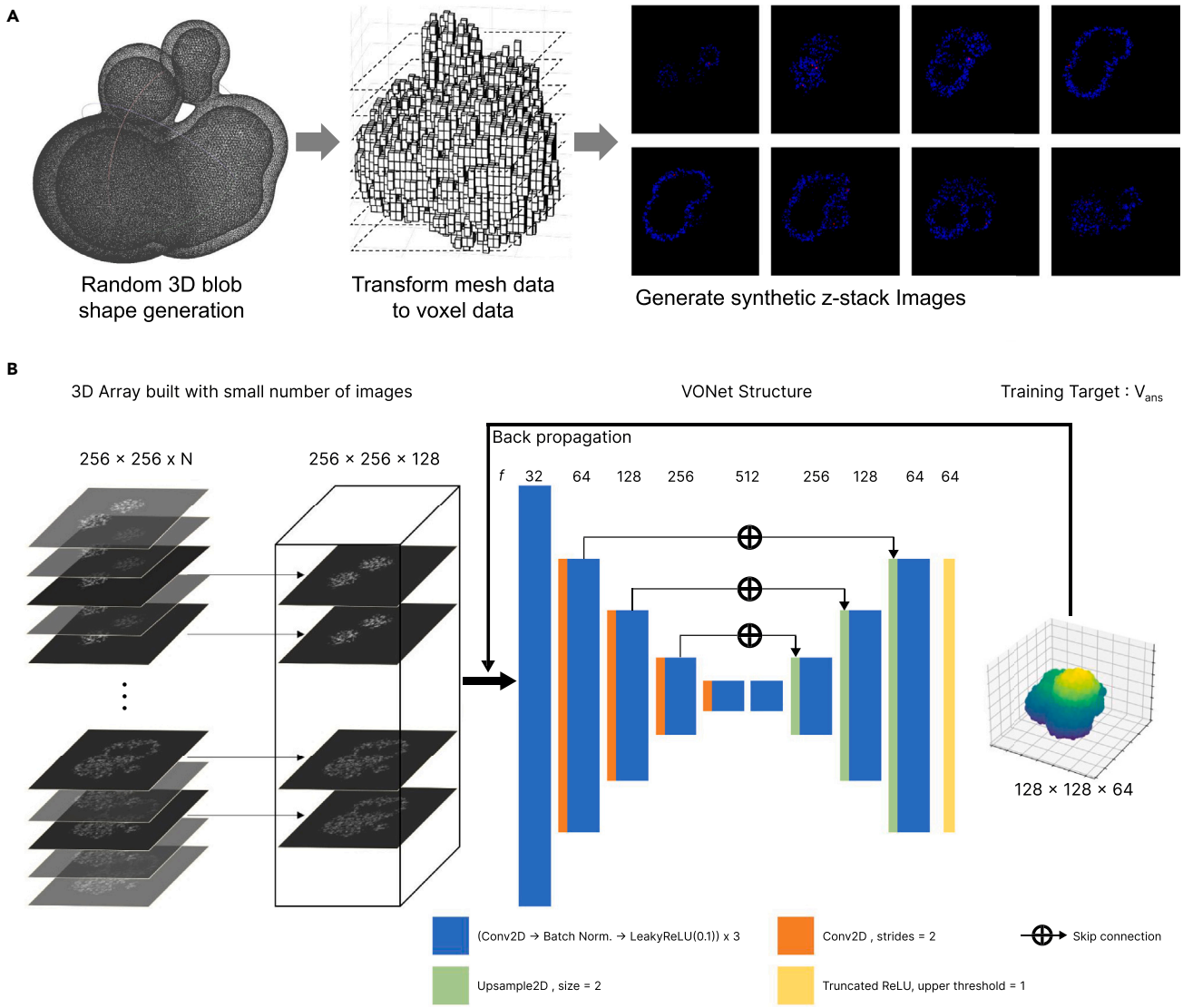

Figure 3. Schematic procedure of VONet

(A) Procedure for creating z stack images of VOs. The mesh data of the VO were transformed into voxel data to create synthetic z stack images.

(B) VONet structure and its training procedure. Single-plane images selected from the 64 z stack VO images were used as input data for VONet. During the data input process for each organoid, 3–19 single-plane images from the whole image set were randomly selected and placed into an input array of the same size.

11 images, which was sufficient for analyzing overall organoid morphology (Figure 5A). IoU_{corr} and IoU_{bright} of $V_{res}(11)$ were >82% (0.82 IoU), on average (Figures 5B and 5C). Notably, $V_{res}(7)$, $V_{res}(9)$, and $V_{res}(11)$ performed significantly better than $V_{res}(13)$ and $V_{res}(15)$. The SD of V_{res} was 0.03–0.05, indicating the robustness of the method.

We compared the voxel data of $V_{res}(5)$, $V_{res}(7)$, $V_{res}(11)$, $V_{res}(15)$, and V_{64} for cultured organoid 608. In Figures 6A–6D, the sky-blue data points represent regions where V_{64} has voxel data but V_{res} does not, while the orange data points represent the opposite. The green data points indicate regions where both V_{res} and V_{64} contain data. Throughout the voxel data, the sky-blue color was mainly observed on the surface of the organoid. As the value of k increased, the area of this region decreased, reaching a minimum at $V_{res}(11)$ (Figure 6C). The orange region significantly decreased when $k \geq 7$ and followed a similar trend to the sky-blue region. The sky-blue and orange regions primarily appeared in the upper portion with high z values, and the number of voxels in the orange region was approximately double that of the sky-blue region (Figure 6E).

We evaluated the differences in the voxel data of $V_{res}(11)$ and V_{64} for the cultured organoids 602 and 603. Differences in the structure of each organoid layer were indicated by the z values from the z stack images, which is shown in Figure 6F. As expected, $V_{res}(11)$ was better at estimating the organoid structure than V_{64} was, based on several cross-sectional superposed images of V_{64} and $V_{res}(11)$ (Figure 6F). Notably, orange regions (V_{res} only) are predominantly observed in data with z values >40, corresponding to deep focal distances. In this range, sky blue regions (V_{64} only) fail to adequately represent the closed

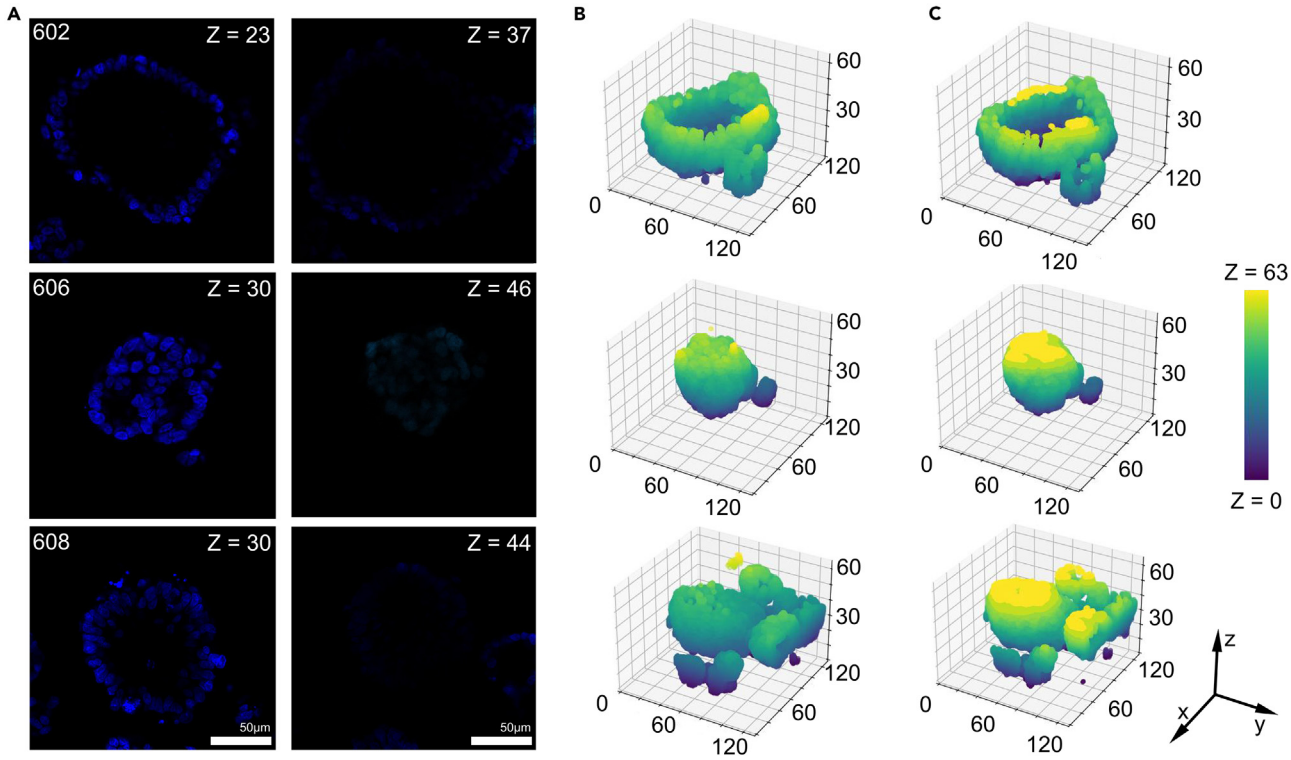

Figure 4. RO dataset and reconstruction of three-dimensional (3D) structure of organoids

(A) z Stack images of the cultured ROs, 602, 605, and 608. As the focal depth of single-plane images increased, the brightness and morphology of the fluorescently stained cell nuclei became increasingly blurred. Scale bar, 50 μm.

(B) The 3D images of these three organoids generated by stacking whole z stack images (64 images) of the cultured organoids (V_{64}).

(C) The 3D images reconstructed using VONet (V_{res}). Eleven z stack images were used for simulation. The invisible area of the deep focal distance was reconstructed via VONet simulation.

structure of the organoids, while orange regions effectively complement this representation. Meanwhile, VONet could not predict the floating nuclei inside the organoid for images of z = 34 and z = 38. We assumed that as the training VO dataset does not contain any small fragments, including debris or a single nucleus in the inner cavity area, VONet cannot estimate the meticulous details of the inner organoid (indicated by arrows). In summary, VONet estimated organoid structural data with a limited number of images, including the invisible area located at a deep focal distance of the organoid, which would be challenging without deep learning. However, VONet exhibited limitations in accurately predicting uncommon structures within organoids, such as floating nuclei.

DISCUSSION

Organoids, 3D cell culture models that closely mimic the structure and functionality of real tissues, have emerged as powerful tools for HCS of drug efficacy and compound toxicity in realistic tissue environments. Unlike conventional 2D cell cultures, organoid models possess volume, necessitating the application of 3D imaging techniques, such as z stack imaging, to analyze their morphological changes. However, traditional confocal microscopy-based z stack imaging is time-consuming, even for single sample acquisition, rendering large-scale HCS studies prohibitively expensive and time-consuming. Consequently, efficient techniques are required to analyze organoid characteristics in HCS platforms.

In this study, we present a deep learning-based 3D organoid rendering system that can reconstruct the entire structure of an organoid from a minimal set of single-plane images with arbitrary focal lengths. To overcome the limitation of insufficient organoid z stack image sets for training deep neural networks, we synthesized around 40,000 organoid z stack images, called VO, to serve as a training dataset. Our VO dataset was designed based on the diverse shapes and growth patterns of cultured organoids and incorporated various components of 3D structure and single-plane image information (mesh, voxels, viability, and z stack image data). The deep learning network trained on the VO dataset, VONet, demonstrated exceptional performance in predicting the entire structure of organoids using a small number of randomly selected z stack images (9–11 images). The performance was validated using a dataset of 10 RO images from cultured samples, confirming its superior predictive ability.

To validate the superiority of VONet in predicting the entire organoid structure from a limited number of single-plane z stack images, we directly compared its performance to traditional image reconstruction methods without deep learning. We used two widely used 3D voxel interpolation methods, bilinear interpolation and second-order B-spline, to predict the 3D structure of

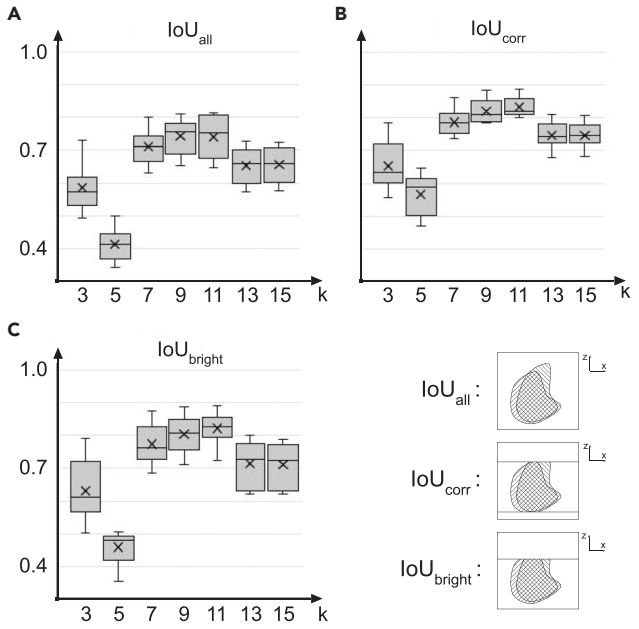

Figure 5. Performance evaluation of the VONet using the IoU criterion

(A) Whisker graph showing the IoU_{all} result of the whole voxel volume.

(B) Whisker graph showing the IoU_{corr} result of the corresponding volume.

(C) Whisker graph showing the IoU_{bright} result measured using z stacks $<0.7 \times z_{max}$. The x axis indicates the variable k value, and the y axis indicates each IoU value. The illustration at right bottom describes the coverage of each IoU criterion.

ROs from a limited number of images (k = 11) and evaluated their similarity to the actual structure using IoU scores. As shown in Table 4, both methods without deep learning (bilinear and B-spline) yielded significantly lower IoU scores compared to our VONet predictions. These results demonstrate that traditional interpolation software is inadequate for 3D organoid structure prediction and highlight the necessity of developing advanced techniques like VONet.

As previously mentioned, conventional z stack image-based 3D structure rendering systems require 60–120 images to reconstruct a single organoid and demand significant processing time. In contrast, VONet efficiently generates 3D organoid structures using only 9–11 single-plane z stack images, making it a valuable tool for commercializing organoid-based HCS platforms. For instance, in a 384-well plate HCS assay, traditional imaging methods would require acquiring 64 single-plane images per organoid, totaling 24,576 images. However, VONet enables reconstruction of the entire 3D organoid structure from only 3,456 images, reducing resource and time consumption by over 85%. We believe this research will significantly contribute to developing high-performance organoid screening systems for novel drug discovery.

The performance of VONet exceeded our expectations in its ability to handle depth-dependent fluorescence signal loss. As shown in Figure 4, single-plane images acquired at deep focal distances using conventional confocal microscopy often suffer from information loss in fluorescence images due to the optical characteristics of the microscope.[8] Interestingly, VONet successfully reconstructed the 3D structure of organoids even when fluorescence signals were missing from deep focal distance images. Alternatively, one could view VONet as simulating the missing z stack image data caused by the limited focal range of confocal fluorescence microscopy. Figure 6 demonstrates that VONet can reasonably infer the morphological features of organoids in regions with missing fluorescence signals in the 3D organoid structure rendering results. We believe that utilizing advanced techniques such as light sheet fluorescence microscopy, which addresses light absorption or scattering issues related to focal range limitations, could further enhance the performance of 3D structure prediction software in future research.

Building 3D voxel and mesh datasets is crucial for analyzing and predicting the 3D morphological features of specific objects using deep learning. However, previous organoid studies have not attempted to construct such datasets. To develop an AI-based organoid structure prediction model, we pioneered the creation of a synthetic dataset representing 3D organoid structures. To ensure the reliability of the synthetic dataset, we devised a method for quantitatively verifying the quality of the synthetic VO used to train VONet. However, since techniques for synthesizing virtual confocal fluorescence microscopy images are not widely established, no well-established standard metrics exist. Therefore, we undertook the task of refining VO quality by breaking down and evaluating image components ourselves.

The VO dataset used in this study is the third iteration, developed through a process of trial and error. The initial VO version 1 lacked many elements necessary for realistic representation of RO images. To enhance the realism of fluorescent microscopy images of nuclei-stained organoids, we refined VO to incorporate various characteristics such as (1) morphological diversity of stained nuclei, (2) speckling patterns of stained nuclei, and (3) spatial distribution of nuclei according to organoid structure. These characteristics were implemented with the same frequency and quality as observed in RO staining images, culminating in the final VO version 3. The synthetic VO data exhibit such a high degree of similarity to real RO data that non-experts cannot distinguish between the two.

The quality of synthetic VO is also highly correlated with the performance of VONet. VONet version 1, trained on the subpar VO version 1, failed to achieve an IoU score of ≥ 0.65 in performance evaluation using the RO dataset. However, VO version 3, which incorporates techniques to enhance the quality of nuclei such as diversifying nucleus shapes using Voronoi tessellation and realistically replicating the speckling patterns of stained nuclei, exhibits remarkable similarity to the morphological features of ROs. As demonstrated in this paper, training VONet using VO version 3 resulted in an IoU score of 0.82 in performance evaluation using the RO dataset. This clearly demonstrates that the higher the quality of single-plane images of synthetic organoids, the better the performance of VONet. It also serves as proof that the quality of VO version 3, as presented in the paper, is sufficient for realizing our technology.

We strongly believe, however, that establishing standardized metrics for quantitatively evaluating the quality of synthetic confocal fluorescence microscopy images is essential for commercializing this technology. As a result, future research related to VO should include investigations into methods for standardizing and quantifying the quality of synthetic images.

Table 1. IoU_{all} derived from the organoid data

Image no.	599	600	601	602	603	604	605	606	607	608	Mean	SD
3	0.525	0.591	0.601	0.494	0.532	0.576	0.669	0.729	0.567	0.563	0.585	0.070
5	0.414	0.341	0.427	0.398	0.490	0.500	0.409	0.419	0.357	0.371	0.413	0.052
7	0.659	0.721	0.734	0.668	0.728	0.702	0.775	0.800	0.629	0.703	0.712	0.052
9	0.675[a]	0.767[a]	0.755[a]	0.693[a]	0.777	0.754	0.795	0.812	0.654[a]	0.737	0.742[a]	0.052[a]
11	0.667	0.687	0.751	0.679	0.787[a]	0.810[a]	0.805[a]	0.814[a]	0.648	0.752[a]	0.740	0.065
13	0.601	0.688	0.694	0.573	0.628	0.623	0.724	0.726	0.586	0.695	0.654	0.058
15	0.605	0.690	0.696	0.575	0.628	0.623	0.725	0.721	0.595	0.702	0.656	0.056

[a]The best result of each organoid.

Despite the remarkable performance of VONet and the well-crafted VO dataset, some intriguing questions remain unanswered. Our analysis reveals that VONet achieves its peak performance when using 9 or 11 single-plane images of organoids. While one might intuitively expect that increasing the number of single-plane images put into VONet would lead to higher structural prediction accuracy, we observed that using 13 or 15 images tends to overestimate the structure of the organoid and yields lower IoU scores compared to 9 or 11 images. The underlying cause of this phenomenon is difficult to pinpoint due to the inherent nature of deep neural networks. However, we hypothesize that it could stem from the imperfections in our synthetic VO data.

ROs, when cultured for extended periods, can undergo morphological changes due to physical forces like gravity. For instance, organoids cultured for a certain duration may exhibit a flattened bottom resembling a mushroom due to gravitational cell compaction. However, our VO dataset does not account for such long-term culture-induced morphological variations, making it an imperfect representation of ROs. We believe that the observed decline in structural prediction accuracy under high data input conditions arises from these imperfections in VO data quality.

To address this issue, future research will focus on developing VO data that more closely resembles ROs. We anticipate that by refining VO quality, we can eliminate this anomaly and further enhance the performance of VONet.

EXPERIMENTAL PROCEDURES

Construction of VOs

The VO recreated the microscopic image of a stained organoid nucleus, which is useful for deriving structural information. The complete VO construction technique can be summarized as follows: (1) creating a random blob with an irregular shape, (2) generating random-shaped nuclei per nucleus point, (3) drawing confocal images according to a given z coordinate. Here, we outline the steps in detail.

Blob generation

The typical structure of an organoid is a blob composed of multiple ellipsoids. We randomized the size, location, and thickness of each ellipsoid to avoid overfitting. The following are the parameters of each ellipsoid used to generate blobs:

$$N : \text{number of ellipsoids in a blob } (1 \le N \le 20)$$

$$E_i : \text{ith ellipsoid in a blob } (1 \le i \le N)$$

$$E_i' : \text{cavity of the ith ellipsoid in a blob that corresponds to } E_i$$

$$x_i, y_i, z_i : x-, y-, z- \text{ coordinate of } E_i \ (-1.0 \le x_i, y_i, z_i \le 1.0)$$

$$x_i', y_i', z_i' : x-, y-, z- \text{ coordinate of } E_i'. \ (x_i - 0.3 \le x_i', \le x_i + 0.3, y_i - 0.3 \le y_i', \le y_i + 0.3, z_i - 0.3 \le z_i', \le z_i + 0.3)$$

$$r_{xi}, r_{yi}, r_{zi} : x/y/z- \text{ axis radius of } E_i \ (0.5 \le r_{xi}, r_{yi}, r_{zi} \le 1.0)$$

$$r_{xi}', r_{yi}', r_{zi}' : x/y/z- \text{ axis radius of } E_{xi}' \ (r_i \times 0.3 \le r_{xi,} \le r_{xi} \times 0.8, r_{yi} \times 0.3 \le r_{yi}', \le r_{yi} \times 0.8, r_{zi} \times 0.3 \le r_{z}', \le r_{zi} \times 0.8)$$

$$a_{xi}, a_{yi}, a_{zi} : x/y/z- \text{ axis rotation angle of } E_i \ (0 \le a_{xi}, a_{yi}, a_{zi} \le 2\pi)$$

$$a_{xi}', a_{yi}', a_{zi}' : x/y/z- \text{ axis rotation angle of } E_i' \ (0 \le a_{xi}', a_{yi}', a_{zi}' \le 2\pi)$$

Here, E'_i is the cavity corresponding to E_i, which expresses the empty space in the RO. All parameters were randomized; however, the ranges of several parameters are dependent on other parameters to generate VO structures representative of ROs. For instance, if r'_{xi} is not dependent on r_{xi}, the cavity becomes larger than an ellipsoid and cannot form the proper blob structure.

Table 2. $IoUc_{orr}$ derived from the organoid data

Image no.	599	600	601	602	603	604	605	606	607	608	Mean	SD
3	0.630	0.639	0.659	0.558	0.577	0.609	0.719	0.786	0.731	0.616	0.652	0.072
5	0.601	0.512	0.469	0.590	0.614	0.571	0.613	0.588	0.645	0.472	0.567	0.062
7	0.792	0.754	0.794	0.754	0.778	0.736	0.836	0.863	0.808	0.752	0.787	0.041
9	0.811	0.807	0.809	0.786	0.816	0.784	0.865	0.884	0.847	0.788	0.820	0.035
11	0.812[a]	0.817[a]	0.816[a]	0.800[a]	0.834[a]	0.826[a]	0.871[a]	0.887[a]	0.856[a]	0.808[a]	0.833[a]	0.029[a]
13	0.726	0.724	0.747	0.680	0.720	0.748	0.778	0.792	0.809	0.737	0.746	0.038
15	0.731	0.725	0.746	0.681	0.720	0.748	0.776	0.790	0.807	0.744	0.747	0.037

[a]The best result of each organoid.

Table 3. IoU_{bright} derived from the organoid data

Image no.	599	600	601	602	603	604	605	606	607	608	Mean	SD
3	0.590	0.611	0.642	0.500	0.537	0.576	0.716	0.791	0.734	0.609	0.631	0.091
5	0.489	0.356	0.485	0.413	0.506	0.502	0.462	0.483	0.473	0.418	0.459	0.048
7	0.743	0.748	0.809	0.685	0.737	0.702	0.845	0.874	0.819	0.774	0.774	0.062
9	0.758	0.798	0.829	0.712	0.784	0.754	0.861	0.886	0.844	0.814	0.804	0.054
11	0.769[a]	0.802[a]	0.842[a]	0.724[a]	0.809[a]	0.810[a]	0.872[a]	0.891[a]	0.852[a]	0.845[a]	0.822[a]	0.050[a]
13	0.688	0.702	0.752	0.621	0.633	0.623	0.784	0.799	0.771	0.758	0.713	0.069
15	0.685	0.703	0.746	0.621	0.633	0.623	0.779	0.790	0.768	0.758	0.711	0.067

[a]The best result of each organoid.

The upper and lower limits of each parameter were arbitrarily determined so that each ellipsoid was randomly distributed but not completely separated from the others. We utilized the Python pyVista module for blob generation (https://docs.pyvista.org/).

Nucleus point generation

First, we determined the number of nuclei in an organoid and the central coordinates of each nucleus (Figure S5). We assumed that the 3D space of an organoid mesh datum has (s, s, s) dimensions. We set the number of the grid spaces to $v \times v \times v = v^3$, where each space has an equal length of $\frac{s}{v}$ and v is a random integer between 26 and 48. A randomized v varies the size of a nucleus so that our dataset covers a broad scale of confocal microscopic images. Each grid space that intersects with the mesh data has only one nucleus, and the initial coordinate of the nucleus point is at the center of the grid space. We added random values *dx* and *dy* to the x, y coordinate values of each nucleus point to avoid the shape and distance between the cells being identical, which causes overfit during learning. Figure S5D shows the quasi-random distribution of the nuclei in the fourth process. A random z coordinate value was applied later. The grid space was then voxelated into two voxels: V_i and V_{64}. V_i has the size of (256 × 256 × 64) and V_{64} has the size of (128 × 128 × 64). V_i was converted to an image set, which was used as input data, and V_{64} was used as the answer voxel data. This conversion allowed the handling of data as images, simplifying further processing. Among the grid center points, those that did not intersect with the mesh became dummy points and were used for the determination of the shape of the nucleus. After setting nucleus points, a live/dead state was randomly imbued to each point. The live/dead rate of the organoid was calculated as the number of live and dead nuclei.

Second, we applied Voronoi tessellation to draw the shape of the nuclei. For every z axis value k ($1 \leq k \leq 64$), a voxel slice S_{vk} of the size (512 × 512) was extracted, and Voronoi tessellation was applied for each slice. Here, both nuclei and dummy points participated in generating random convex blobs that resembled the real nuclei. After tessellation, we applied Gaussian smoothing-thresholding iteratively to generate a smooth-curved random 2D blob image with certain fixed threshold values; the number of iterations can determine the final size of the nucleus (Figure S5F). For live nuclei, smoothing-thresholding was applied three times. As dead nuclei are smaller than live nuclei, we set the number of iterations for dead nuclei to a random number between 5 and 7. The resulting image was called I_{bn}, representing the nucleus image of the nth cell. The overall process is shown in Figures S5A–S5F.

Confocal image drawing and answer voxel generation

According to Svoboda et al.,[24] combining Perlin and fractal noise in one image is adequate to mimic the inner structure of a nucleus (chromatin, lysosome, and mitochondrion). After observing the nuclei, we generated an edge image of I_{bn} to realistically simulate confocal microscopic images. Extracting the edge from I_{bn} using the simple Sobel filter[25] generates edge image I_{en}, which represents the nucleus envelope. Then, both I_{bn} and I_{en} were multiplied with a 2D Perlin noise and a 2D fractal image. Summing I_{bn} and I_{en} gave the final single nucleus image I_{cn}, which was randomly produced for every central nucleus point. This process is shown in Figure S5G.

To create a realistic set of images, we slightly varied the center point coordinate of each nucleus along the z axis and imbued the volumetric information. The initial coordinate of one nucleus was $X_n = \{x_n, y_n, z_n\}$, where x_n, y_n, and z_n are integers. If a nucleus is alive, the modified coordinate becomes $X_{nl} = \{x_n, y_n, z_n + dz\}$, where dz is a random integer between −2 and 2.

In the case of an RO, a dead nucleus tends to fall off and float in the liquid medium or sink to the bottom of the plate. To simulate this, the coordinate of the dead nucleus X_{nd} became

$$X_{nd} = \{x_n + dx' \times P_f(X_{nd}), y_n + dy' \times P_f(X_{nd}), z_n + dz' \times P_f(X_{nd})\}(dx^2 + dy^2 = r_n)$$

$$P_f(X_{nd}) = \begin{cases} 1\ (rnd_n \leq lrd) \\ 0\ (rnd_n > lrd) \end{cases}$$

$$0 \leq r_n \leq 80 \times lrd$$

$$0 \leq dz \leq k$$

Here, rnd_n is a random positive real number <1.0 that determines whether a nucleus is alive or dead. If rnd_n is smaller than lrd, the nucleus is alive. r_n indicates the maximum distance of a dead nucleus from its initial position.

Next, we selected the height of each nucleus in V_i and made the plain nuclei volumetric. According to our observations of organoid images, one live nucleus appeared in 6–10 consecutive slices. We randomly imbued the height value to each nucleus and filled the neighboring slice images to generate the confocal microscopy image set using I_{cn}. Suppose that we generate an image of a slice with k = 48 (S_k) and the height of the nucleus corresponds to slice number 7, then the image of the nucleus is scaled and copied to slices with k′ ($45 \leq k' \leq 51$), where k′ is a z value near slice S_k. To approximate an oval shape, the image that will be copied to the neighbor slice becomes

$$I_{cnk'} = \text{Scale}\,(s, I_{cn})$$

$$s = \frac{1}{k - k'^2}$$

where the function Scale () is equal to function cv2.resize() of the openCV library (https://opencv.org/). The transformed image $I_{cnk'}$ was drawn on $S_{k'}$ to complete the voxel data. The process and its results are shown in Figure S6.

The final step is the answer voxel data and final confocal microscopic images generation. Suppose that we want to generate an image of a slice that has three nuclei with different center coordinates. If the center of a nucleus is on the plane of interest, then I_{cn} or $I_{cnk'}$ can be included in the slice image without postprocessing. For nuclei on the left side, the z axis distance between S_k and $S_{k'}$ is $k - k' = 3$. We adjusted the Gaussian blur filter ($k - k'$) times on I_{cn} to mimic the out-focused confocal image. The process and resulting VO image are shown in Figure S7.

We found that the mean intensity of the nuclei in real confocal microscopic images linearly decreased to near 0 as the z value increased. To imitate this, we multiplied all slice images by (1–0.0156k) (Figure S8).

The answer voxel data were obtained by resizing V to (128 × 128 × 64) and setting the intensity of all non-zero voxel points to 1, corresponding to V_{64}. The 3D voxel data require a large amount of memory at high resolutions. For example, for 3D voxel data generated from a standard confocal image set without any preprocessing, the size of input/output data becomes (512 × 512 × 64), which cannot be handled by standard computing devices. We selected (128 × 128 × 64) as the size of the final data, which is common for deep learning models

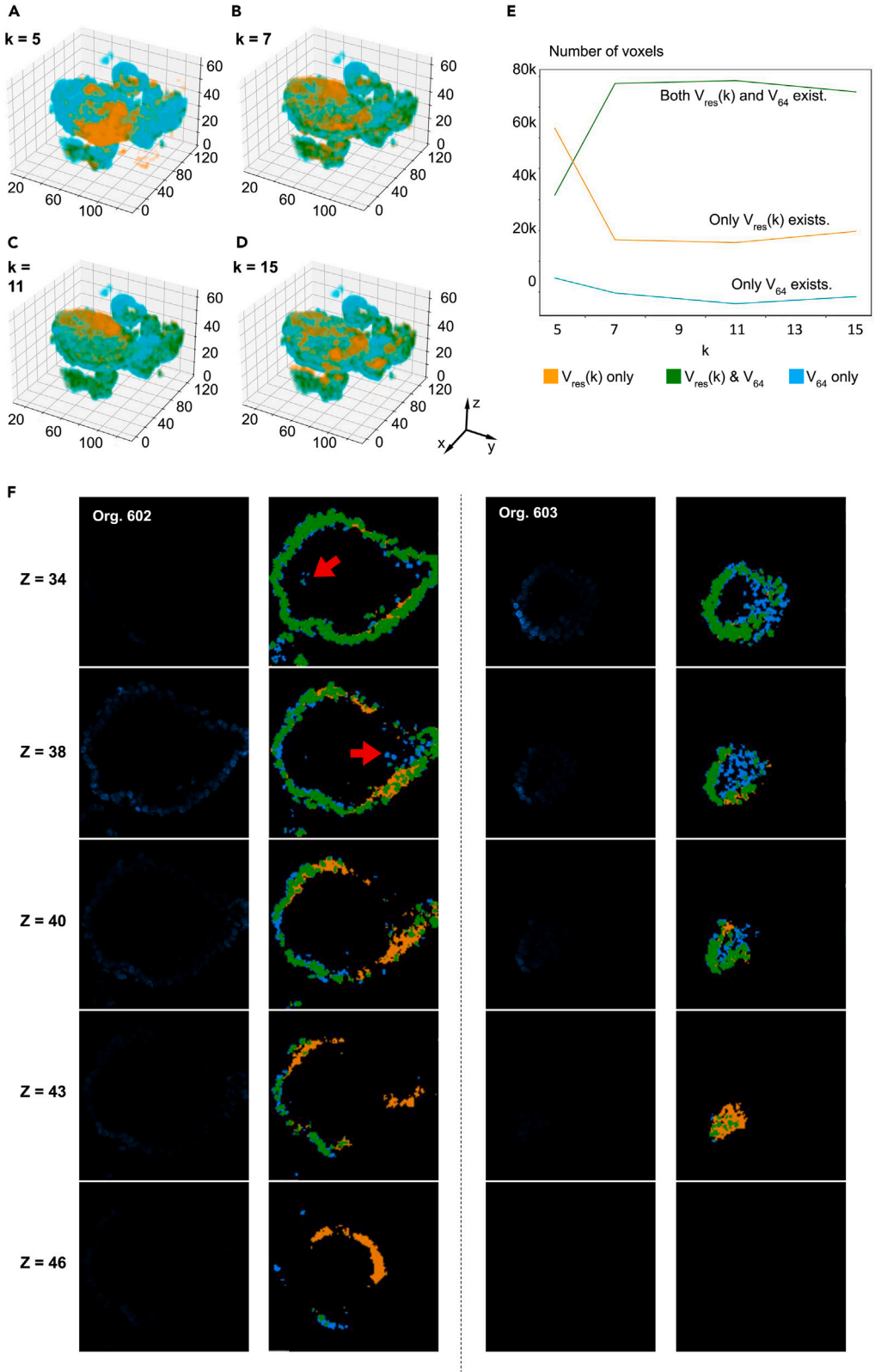

(legend on next page)

using 3D voxel data. Although this size sacrifices some information, it remains suitable for shape analysis. At this point, we used the synthesized confocal microscopy image set and 3D data to train a deep learning network.

Deep learning for organoid reconstitution

The main structure of our network is similar to U-net-like, but with fewer skip connections owing due to the size disparity between the input and output. We extracted only blue channel images for training as only live nuclei can sustain the structure of an organoid.

Unlike other 3D data processing deep learning networks, we employed a 2D-convolutional network to predict the structure of an organoid from a stack of several images, which requires height information for robust prediction performance. We empirically demonstrated that simply stacking a fixed number of images/adjusting several Siamese networks on images was ineffective. An empty array A with dimensions (256 × 256 × 64) was created, and each slice of the array was filled with a confocal microscopy image that had the same z value. For example, suppose that you want to use three images as input and the z value of each slice is 10, 30, and 50. We can then write each image as $I_{z=10}$, $I_{z=30}$ I, and $I_{z=50}$ and fill A as follows:

$$A_{z=10} = I_{z=10}$$

$$A_{z=30} = I_{z=30}$$

$$A_{z=50} = I_{z=50}$$

where $A_{z=k}$ denotes the slice of A that is located at *k* along the z axis. However, setting up the input in this way creates large cavities that correspond to (1 – k/64) × 100% of A. For example, if you want to use only three images as input, 95.3% of A has no data and 4.7% is planar. Considering the volume covered by the 3D convolutional layer, adjusting 3D convolution on A will make the filter consider only the blank volume and fail to optimize the weight of the model. In contrast, adjusting the 2D convolutional layer generates a 2D image that has 64 color channels. In this case, the deep learning network always considers non-zero data, ensuring the weights converge. The difference between the 2D and 3D convolution is shown in Figure S9: the filter of the 3D convolution refers to the volume that has no data, whereas the filter of the 2D convolution is always able to utilize non-zero data.

The pre-processing of the input data and structure of the network are shown in Figure S9. To enable the use of the network with an arbitrary number of images, we chose the number of images to upload at random. As the size of the input was always 64, regardless of the number of images, no additional post-processing programming was required. The number of images N ranged from 1 to 21, and the distance between adjacent slices was set to 64/N. We set N to always be an odd number to ensure that data always exist in slices with z = 32. The process of preparing the input array is shown in Figure S10.

We observed that input arrays with a fixed number of images never converge. When the number of images is fixed, slices that lack an image in the input array are left blank, resulting in N ring-shaped output data. We inferred that randomizing the size of the space between slices prevents the network from overfocusing on specific slices because our input setting dynamically alters the location where data exist with respect to N, thereby assisting the network in adapting to different input conditions. Instead of using the Softmax or Sigmoid function as the final activation layer, which failed to converge, we used a truncated ReLU function layer. Our final network contains 23.3 million weights.

Normal colon and cancer organoid cultures for benchmark dataset

After dissolving patient-derived normal colon and cancer organoids stored in LN2, they were suspended in 9 mL washing medium containing DMEM/F12 (Corning, Corning, NY) supplemented with penicillin/streptomycin and knockout serum (Gibco, Waltham, MA). The suspension was centrifuged at 450 × *g* for 3 min. Following centrifugation, the supernatant was removed, and the cell pellet was resuspended in Matrigel (Corning). The resuspended cells were then seeded and solidified as a Matrigel droplet in a multi-well plate at 37°C for 10 min.

After the Matrigel solidified, a colon organoid-specific culture medium was added. This medium consisted of advanced DMEM/F12 with penicillin/streptomycin, 1× B27, N2, GlutaMAX, 10 mM HEPES (Gibco), 10 mM nicotinamide, 1.25 mM *N*-acetyl-L-cysteine, 10 nM gastrin, 500 nM A83-01, 50 μg/mL gentamicin (Sigma-Aldrich, St. Louis, MO), 50 ng/mL recombinant human (rh) epidermal growth factor, 50 ng/mL fibroblast growth factor-basic, 1 μg/mL rhR-spondin-1, 100 ng/mL rhNoggin (PeproTech, Hamburg, Germany), 100 ng/mL insulin-like growth factor 1 (BioLegend, San Diego, CA), 100 ng/mL rhWnt3a (R&D Systems, Minneapolis, MN), 50 μg/mL Primocin (Invivogen, Toulouse, France), and 10 μM ROCK inhibitor (Y-27632; PeproTech).

The medium was replaced every 2 days, and organoids were passaged weekly. The 3D organoids were cultured for several days until they developed a stable and diverse morphology. Images of the organoid growth patterns were captured using a Primovert inverted microscope (Carl Zeiss, Oberkochen, Germany) and processed with Zen 3.0 software (Carl Zeiss).

Sampling and immunocytochemistry

To sample organoids, the Matrigel droplet containing the organoids was gently pipetted to break it up and then carefully collected into a conical tube. The organoids were washed with cold PBS and resuspended in a cell recovery solution (Corning) to remove any remaining Matrigel. The collected organoids were then fixed with 4% paraformaldehyde for 1 h. Next, they were permeabilized with 0.1% Triton X-100 in Dulbecco's PBS containing 0.2% BSA (Sigma-Aldrich) for 15 min to prepare for nucleus staining.

The organoid nuclei were stained with DAPI (1:4,000, Thermo Fisher Scientific, Waltham, MA) for 30 min at 25°C. After staining, the organoids were washed three times with 0.1% PBST. Finally, the stained organoids were transferred to a confocal dish for imaging.

Confocal imaging

Images of the organoids were captured using an LSM800 confocal microscope (Carl Zeiss) and processed with Zen 3.0 software (Carl Zeiss). Full 3D images of the nucleus-stained organoids were generated from a series of 64 single planes, each with a thickness of 2 μm, using a z stack imaging tool.

Dataset description and experimental setup

Our VO dataset had 39,633 organoids, and the total number of images was 2.54 million, 95% of which were used in training and 5% in validation. Image resolution was (512 × 512) and was resized to (256 × 256) for use as input. The initial training rate was 0.001 and reduced by half per 5 epochs. The network was trained for 100 epochs with Adam optimization and a batch size of 8. We used Tensorflow (https://www.tensorflow.org/) and Keras (https://keras.io/) for training, with 128 GB RAM and 32 GB VRAM (Nvidia TeslaV100, Nvidia, Santa Clara, CA). Each training epoch took 4–5 h; the amount of data was so large that we used a partial data load library implemented as a Tensorflow Sequence library (https://www.tensorflow.org/api_docs/python/tf/keras/utils/Sequence).

RESOURCE AVAILABILITY

Lead contact

Further information and requests for resources should be directed to and will be fulfilled by the lead contact, Taehwan Kwak (taehwan.kwak@nextandbio.com).

Figure 6. Voxel data comparison between V_{res} (k) and V_{64}

(A–D) Visualization of the derivation results overlapping the voxel data of V_{res} (k) and V_{64} derived from the organoid 608. (A) $V_{res}(5)$ and V_{64}; (B) $V_{res}(7)$ vs. V_{64}; (C) $V_{res}(11)$ vs. V_{64}; and (D) $V_{res}(15)$ vs. V_{64}. The sky-blue region indicates the area with V_{64} data but without V_{res} data, and the orange region indicates the reverse. The green region denotes that both V_{res} and V_{64} have data.

(E) Graph showing the number of voxel data of $V_{res}(k)$ of the organoid 608.

(F) Comparison between the voxel data of V_{res} (11) and V_{64} of the organoids 602 and 603 organoids. Left columns of each organoid show the z stack images on each z value. Right columns of each organoid show the cross-sectional images overlapping with the voxel data of $V_{res}(11)$ and V_{64}.

Table 4. Comparison of VONet performance with existing 3D structure prediction techniques

	IoU score		
Organoid no.	Bilinear	Second-order B-spline	VONet $V_{res}(11)$
599	0.448	0.449	0.769
600	0.420	0.420	0.802
601	0.444	0.444	0.842
602	0.395	0.398	0.724
603	0.448	0.455	0.809
604	0.439	0.447	0.810
605	0.445	0.443	0.872
606	0.445	0.444	0.891
607	0.417	0.417	0.852
608	0.381	0.378	0.845

Materials availability

This study did not generate new unique reagents.

Data and code availability

All of the VONet code and image datasets for structure reconstruction and analyses in this paper are publicly available online in a Zenodo repository.[26] The VO dataset used for training and validating VONet includes over 39,000 samples, making the dataset too large to be fully shared through a public repository. Consequently, only 50 samples from the VO image set have been made available in a public repository. Researchers wishing to access the complete dataset should communicate with the lead contact via e-mail. Access to the data stored on the institution's web server will be granted, enabling the download of the entire dataset.

ACKNOWLEDGMENTS

This work was supported by the Technology Innovation Program (20009125, Drug Efficacy and Toxicity Screening on Microenvironment Integrated Uniform Organoids) and the Technology Innovation Program (20009853, Establishment of a High-Content 3D Organ-on-a-Chip System for Studying Pancreatic Disease Modeling *In Vitro*). Both programs are funded by the Ministry of Trade, Industry and Energy (MOTIE, Korea).

AUTHOR CONTRIBUTIONS

E.S. conceived and designed the study, performed the experiments, and participated in manuscript writing. M.K., S.L., H.-W.L., D.-H.C., and J.K. performed the experiments and collected and/or assembled the data. R.K. and J.H.Y. analyzed and interpreted the data. S.C. and T.H.K. conceived and designed the study, analyzed and interpreted the data, and participated in manuscript writing. All authors approved the final version of the manuscript.

DECLARATION OF INTERESTS

The authors declare no competing interests.

SUPPLEMENTAL INFORMATION

Supplemental information can be found online at https://doi.org/10.1016/j.patter.2024.101063.

Received: January 3, 2024
Revised: May 29, 2024
Accepted: August 29, 2024
Published: September 30, 2024

REFERENCES

1. Kim, J., Koo, B.K., and Knoblich, J.A. (2020). Human organoids: model systems for human biology and medicine. Nat. Rev. Mol. Cell Biol. *21*, 571–584. https://doi.org/10.1038/s41580-020-0259-3.
2. Zhao, Z., Chen, X., Dowbaj, A.M., Sljukic, A., Bratlie, K., Lin, L., Fong, E.L.S., Balachander, G.M., Chen, Z., Soragni, A., et al. (2022). Organoids. Nat. Rev. Methods Primers *2*, 94. https://doi.org/10.1038/s43586-022-00174-y.
3. Aberle, M.R., Burkhart, R.A., Tiriac, H., Olde Damink, S.W.M., Dejong, C.H.C., Tuveson, D.A., and van Dam, R.M. (2018). Patient-derived organoid models help define personalized management of gastrointestinal cancer. Br. J. Surg. *105*, e48–e60. https://doi.org/10.1002/bjs.10726.
4. Matthews, J.M., Schuster, B., Kashaf, S.S., Liu, P., Ben-Yishay, R., Ishay-Ronen, D., Izumchenko, E., Shen, L., Weber, C.R., Bielski, M., et al. (2022). OrganoID: A versatile deep learning platform for tracking and analysis of single-organoid dynamics. PLoS Comput. Biol. *18*, e1010584. https://doi.org/10.1371/journal.pcbi.1010584.
5. Beck, L.E., Lee, J., Cote, C., Dunagin, M.C., Lukonin, I., Salla, N., Chang, M.K., Hughes, A.J., Mornin, J.D., Gartner, Z.J., et al. (2022). Systematically quantifying morphological features reveals constraints on organoid phenotypes. Cell Syst *13*, 547–560.e3. https://doi.org/10.1016/j.cels.2022.05.008.
6. Rezakhani, S., Gjorevski, N., and Lutolf, M.P. (2021). Extracellular matrix requirements for gastrointestinal organoid cultures. Biomaterials *276*, 121020. https://doi.org/10.1016/j.biomaterials.2021.121020.
7. Chen, S., Zhao, M., Wu, G., Yao, C., and Zhang, J. (2012). Recent advances in morphological cell image analysis. Comput. Math. Methods Med. *2012*, 101536. https://doi.org/10.1155/2012/101536.
8. Elliott, A.D. (2020). Confocal Microscopy: Principles and Modern Practices. Curr. Protoc. Cytom. *92*, e68. https://doi.org/10.1002/cpcy.68.
9. Dekkers, J.F., Alieva, M., Wellens, L.M., Ariese, H.C.R., Jamieson, P.R., Vonk, A.M., Amatngalim, G.D., Hu, H., Oost, K.C., Snippert, H.J.G., et al. (2019). High-resolution 3D imaging of fixed and cleared organoids. Nat. Protoc. *14*, 1756–1771. https://doi.org/10.1038/s41596-019-0160-8.
10. Lukonin, I., Zinner, M., and Liberali, P. (2021). Organoids in image-based phenotypic chemical screens. Exp. Mol. Med. *53*, 1495–1502. https://doi.org/10.1038/s12276-021-00641-8.
11. Daugherty, R.L., Serebryannyy, L., Yemelyanov, A., Flozak, A.S., Yu, H.J., Kosak, S.T., deLanerolle, P., and Gottardi, C.J. (2014). α-Catenin is an inhibitor of transcription. Proc. Natl. Acad. Sci. USA *111*, 5260–5265. https://doi.org/10.1073/pnas.1308663111.
12. Steigele, S., Siegismund, D., Fassler, M., Kustec, M., Kappler, B., Hasaka, T., Yee, A., Brodte, A., and Heyse, S. (2020). Deep Learning-Based HCS Image Analysis for the Enterprise. SLAS Discov. *25*, 812–821. https://doi.org/10.1177/2472555220918837.
13. Choi, D.H., Liu, H.W., Jung, Y.H., Ahn, J., Kim, J.A., Oh, D., Jeong, Y., Kim, M., Yoon, H., Kang, B., et al. (2023). Analyzing angiogenesis on a chip using deep learning-based image processing. Lab Chip *23*, 475–484. https://doi.org/10.1039/d2lc00983h.
14. Ronneberger, O., and Fischer, P. (2015). Brox T.U-net: Convolutional networks for biomedical image segmentation Medical Image Computing and Computer-Assisted Intervention – MICCAI, pp. 234–241. 201523951. https://doi.org/10.1007/978-3-319-24574-4_28.
15. Yang, L., Ghosh, R.P., Franklin, J.M., Chen, S., You, C., Narayan, R.R., Melcher, M.L., and Liphardt, J.T. (2020). NuSeT: A deep learning tool for reliably separating and analyzing crowded cells. PLoS Comput. Biol. *16*, e1008193. https://doi.org/10.1371/journal.pcbi.1008193.
16. Saood, A., and Hatem, I. (2021). COVID-19 lung CT image segmentation using deep learning methods: U-Net versus SegNet. BMC Med. Imaging *21*, 19. https://doi.org/10.1186/s12880-020-00529-5.
17. Zhang, J., Zhang, Y., and Xu, X. (2021). Pyramid U-Net for Retinal Vessel Segmentation. IEEE Int Conf Acoust Speech Signal Process, 1125–1129. https://doi.org/10.1109/icassp39728.2021.9414164.

18. Fakhry, A., Zeng, T., and Ji, S. (2017). Residual Deconvolutional Networks for Brain Electron Microscopy Image Segmentation. IEEE Trans. Med. Imaging *36*, 447–456. https://doi.org/10.1109/TMI.2016.2613019.

19. Rombach, R., Blattmann, A., Lorenz, D., Esser, P., and Ommer, B. (2021). High-resolution image synthesis with latent diffusion models. arXiv. https://doi.org/10.48550/arXiv.2112.10752.

20. Ramesh, A., Dhariwal, P., Nichol, A., Chu, C., and Chen, M. (2022). Hierarchical text-conditional image generation with clip latentspreprint at arXiv. https://doi.org/10.48550/arXiv.2204.06125.

21. Cho, E.J., Kim, M., Jo, D., Kim, J., Oh, J.H., Chung, H.C., Lee, S.H., Kim, D., Chun, S.M., Kim, J., et al. (2021). Immuno-genomic classification of colorectal cancer organoids reveals cancer cells with intrinsic immunogenic properties associated with patient survival. J. Exp. Clin. Cancer Res. *40*, 230. https://doi.org/10.1186/s13046-021-02034-1.

22. Driehuis, E., Gracanin, A., Vries, R.G.J., Clevers, H., and Boj, S.F. (2020). Establishment of Pancreatic Organoids from Normal Tissue and Tumors. STAR Protoc. *1*, 100192. https://doi.org/10.1016/j.xpro.2020.100192.

23. Kim, M., Mun, H., Sung, C.O., Cho, E.J., Jeon, H.J., Chun, S.M., Jung, D.J., Shin, T.H., Jeong, G.S., Kim, D.K., et al. (2019). Patient-derived lung cancer organoids as in vitro cancer models for therapeutic screening. Nat. Commun. *10*, 3991. https://doi.org/10.1038/s41467-019-11867-6.

24. Svoboda, D., Kozubek, M., and Stejskal, S. (2009). Generation of digital phantoms of cell nuclei and simulation of image formation in 3D image cytometry. Cytometry A. *75*, 494–509. https://doi.org/10.1002/cyto.a.20714.

25. Kanopoulos, N., Vasanthavada, N., and Baker, R.L. (1988). Design of an image edge detection filter using the Sobel operator. IEEE J. Solid-State Circuits *23*, 358–367. https://doi.org/10.1109/4.996.

26. Kwak, T.H. (2024). VOnet codes and organoid single-plane image datasets (Version v3.0.0) [Data set]. Zenodo. https://doi.org/10.5281/zenodo.13131781.